Chapter 6

An Efficient Algorithm for the MGE Fit of Galaxy Images[1]

Abstract

In this Chapter we describe a simple, yet efficient, robust and fully automatic algorithm for the determination of a Multi Gaussian Expansion (MGE) fit to galaxy images, to be used as a parametrization for the galaxy stellar surface density. In most cases it can be verified that the least-squares solution found by this method essentially corresponds to the *minimax* MGE approximation of the galaxy surface brightness, with the chosen number of Gaussians. This algorithm is here specialized for the case of Gaussians with the same center and position angle, and is well suited to be used with multiple resolution images (e.g. HST and ground-based). It works orders of magnitude faster and is more accurate that a brute-force solution of the problem. An alternative fully linear algorithm, that is *guaranteed* to converge to the smallest χ^2 solution, is also discussed.

6.1 Introduction

The original idea of the application of the Multi Gaussian Expansion (MGE) method to the problem of the deconvolution and deprojection of galaxy images comes from Bendinelli (1991). This idea has been generalized for the non-spherical case and made applicable to real galaxies by Monnet, Bacon & Emsellem (1992) and further developed by Emsellem, Monnet & Bacon (1994) and Emsellem, Dejonghe & Bacon (1999).

The MGE method simply consists in a series expansion of galaxy images using bidimensional (2D) Gaussian functions. The Gaussians have the beneficial properties that both the convolution (e.g. to take seeing or PSF effects into account) and the deprojection (to derive the intrinsic stellar luminosity density from the observed galaxy photometry[2]) can be performed analytically in a simple and efficient manner. As shown by Emsellem et al. (1994), many other dynamical and photometric quantities can be evaluated more easily and accu-

[1]Cappellari, M. 2000 in preparation

[2]The deprojection is formally unique *under the MGE assumptions* for an axisymmetric object, but even in this case it will represents one of the possible solutions to this intrinsically non-unique inversion problem (Rybicki, 1986). Once an inclination has been adopted, regularization could be analytically imposed on the MGE intrinsic density, during the fitting process, to further constrain the solution.

rately when the density is expressed in MGE form. For example the MGE potential can be computed with a single integration, as opposed to the two that are required in a general case, when the intrinsic density is stratified on similar triaxial ellipsoids. In the case of $f(E, L_z)$ axisymmetric MGE dynamical models the velocity moments predicted from Jeans equations, already projected onto the sky, can be expressed with only a double integration. The even part of the distribution function can also be more easily retrieved from an MGE density distribution via the Hunter & Quian (1993) formalism.

The MGE parametrization is currently one of the few simple parametrization that are general enough to reproduce the surface brightness of realistic multicomponent objects (e.g. spirals with multiple disks) and has been already adopted for the modeling of a number of galaxies (Emsellem et al., 1994, 1996, 1999; Emsellem, 1995; van den Bosch et al., 1998; Cretton & van den Bosch, 1999).

What is however still missing from the MGE machinery is an accurate, easy to use, generally available, robust and automatic algorithm for the determination of an MGE expansion from galaxy images. In this Chapter we present that algorithm, here specialized to the case of centered Gaussians with the same position angle. This is what is needed for the modeling of general axisymmetric bodies, or triaxial ones in which the density is assumed to be stratified on similar ellipsoids.

6.2 MGE Fitting

6.2.1 The Brute-Force 2D Approach

The determination of an axisymmetric MGE parametrization from the photometry, namely the fit of a sum of Gaussians with the same center and position angle, to a galaxy image seems a very simple problem that can be efficiently solved with general bound constrained nonlinear minimization algorithm.

In what follows we assume for simplicity that the position angle of all Gaussians is known and is parallel to the x axis[3]. The MGE analytic expression for the galaxy surface density[4], is given by

$$\Sigma(x, y) = \sum_{i=1}^{N} P'_i \exp\left[-\frac{1}{2\sigma_i^2}\left(x^2 + \frac{y^2}{q'^2_i}\right)\right], \tag{6.1}$$

where N is the number of the adopted Gaussian components, having central surface density P'_i, observed axial ratio q'_i and dispersion σ_i along the major axis. The straightforward MGE fit approach consists in fitting the nonlinear function $\Sigma(x, y)$ to the pixels of the image by minimizing the χ^2 (pixel binning can be taken into account in the very innermost few pixels)

$$\chi^2 = \sum_{i,j}\left[\frac{I_{i,j} - \Sigma(x_i, y_j)}{\Delta_{i,j}}\right]^2, \tag{6.2}$$

where $I_{i,j}$ are the pixel counts, $\Delta_{i,j}$ is the corresponding photometric error and the sum is

[3]We don't fit the position angle since it is very easily measured before the fit. We found it fast and accurate to determine it from the weighted second moments of the surface brightness above a given level. It may also be measured with standard photometric programs.

[4]We assume the Gaussians are previously analytically convolved with the PSF (e.g., Monnet et al., 1992, Equation (28))

done over all (good) image pixels. Positivity constraint are generally enforced on the P_i', although in principle only the total surface density needs to be positive everywhere.

Although the convergence can be improved by starting the fit with few Gaussians and then adding new components as long as the residuals decrease appreciably (Emsellem et al., 1994), we have discovered that this brute force approach does not work well in practice for two main reasons:

- the nonlinear function χ^2 above presents a large number of local stationary points. In fact suppose that we have found a minimum of the χ^2 with N Gaussians. A new configuration with $N+1$ Gaussians, where the new Gaussian is equal to one of those previously found, is a saddle point for the χ^2. Consequently even state of the art nonlinear fitting algorithm have a high chance of stopping or slowing down considerably in a narrow valley in the $3N$-dimensional space (with $N \approx 10-15$) close to one of these many stationary points, unless the initial guess is very near to the true minimum;

- the "correct" weighting of the pixel measurements tend to produce a model that underestimate the nuclear density due to the fact that the total χ^2 of Equation (6.2) is dominated by the contribution of many pixels at large radii. This is *not* what is needed for an accurate dynamical model of the nucleus.

The net result is that using the above approach the process proceeds by trial and error, with a lot of manual intervention. An automatic fit generally takes many hours on a 333 MHz PC and often converges to a solution that can obviously still be manually improved.

6.2.2 An Efficient 1D Algorithm

To solve this situation we start by analyzing the peculiarities of an MGE fit to a one-dimensional (1D) profile, as can be obtained by measuring the photometry of a galaxy with constant ellipticity. Since galaxy profiles are generally well described by multiple power-law regimes (e.g. Lauer et al., 1995), in this section we start by trying to satisfy the natural requirement that the fit has to "looks good" on a log-log plot (e.g. Byun et al., 1996; Gebhardt et al., 1996). To obtain this result we do the following:

- we sample the profile logarithmically in radius. This is usually done in galaxy photometry to improve the S/N at large radii while still maintaining all the information at the smaller radial scales;

- we require the fit to optimize the *relative* error, namely we minimize

$$\chi^2 = \sum_{i=1}^{M} \left[\frac{I_i - \Sigma(R_i)}{\Sigma(R_i)} \right]^2, \tag{6.3}$$

  where M is the number of photometric data points I_i in the profile, R_i is the corresponding isophote major axis and $\Sigma(R)$ is the 1D version of Equation (6.1).

The reason why Gaussians are so successful in reproducing power-law profiles lies in the fact that every Gaussian provides a very localized contribution to the profile, only for radii close to its σ_i. In fact 1) at small radii ($R \ll \sigma_i$) Gaussians becomes very rapidly constant, while power-laws continue to rise, 2) at large radii ($R \gg \sigma_i$) Gaussians go to zero much

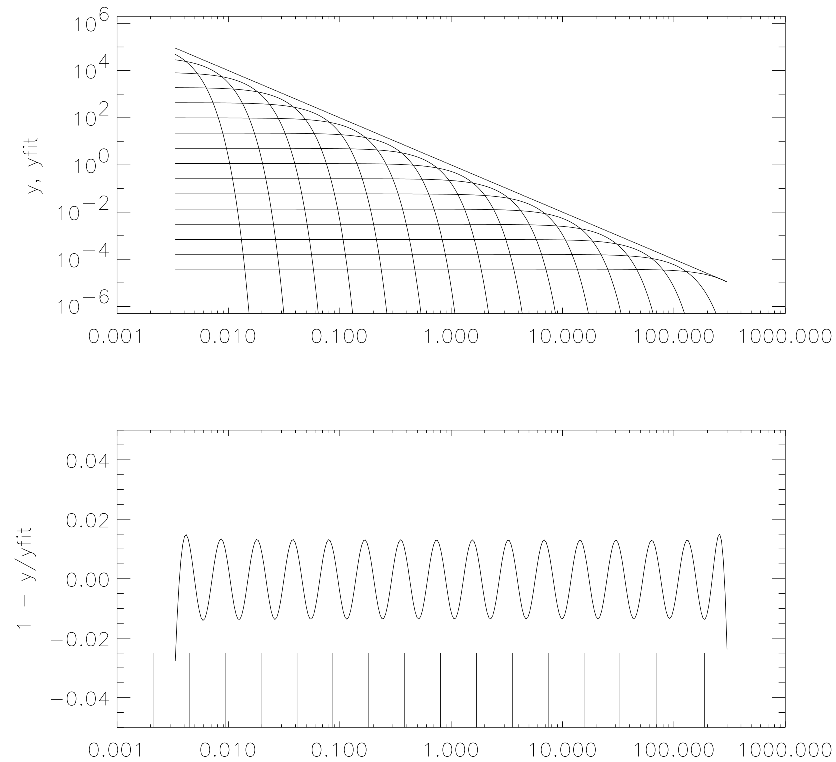

Figure 6.1: 1D MGE fit to the power-law profile R^{-2}. *Top panel:* the profile and the $N = 16$ best fitting Gaussians components are shown. *Bottom panel:* radial variation of the relative error in the profile fit. Note that the maximum error is reached precisely $2N + 1$ times, with alternating signs. The vertical lines indicate the σ_i of the Gaussians shown in the upper panel.

more rapidly than a power-law. It appears clear that the MGE best fitting solution for a logarithmically sampled power-law profile consists in a series of Gaussians that are also logarithmically spaced, both in σ_i and in height P'_i, within the ranges imposed by the data (see Figure 6.1).

We now show that this solution is the true *global* minimum. In fact it can be demonstrated that the unique *minimax*[5] MGE approximation, with positive Gaussians, to a given decreasing function of radius, in a given interval, is characterized by the condition that the maximum relative error is reached precisely $2N + 1$ times, with alternating signs. A similar condition also exists for other approximating functions e.g. Chebyshev polynomials and rational functions (see e.g. Press et al., 1992). From the fact that this condition is also satisfied in our least-squares solution we know that our algorithm is able to converge to the minimax MGE approximation of a power-law. The same condition can be verified in the case of more realistic profiles composed by multiple power-law regimes (Figure 6.2), and essentially for any function that appears smooth in a log-log plot. Here the Gaussians will not be precisely logarithmically spaced in the σ_i, but will be more closely spaced where the profile is more cuspy (Figure 6.3). Also in these cases however our least-squares solution essentially provides the minimax MGE approximation of the given function.

[5]The solution minimizing the maximum absolute error.

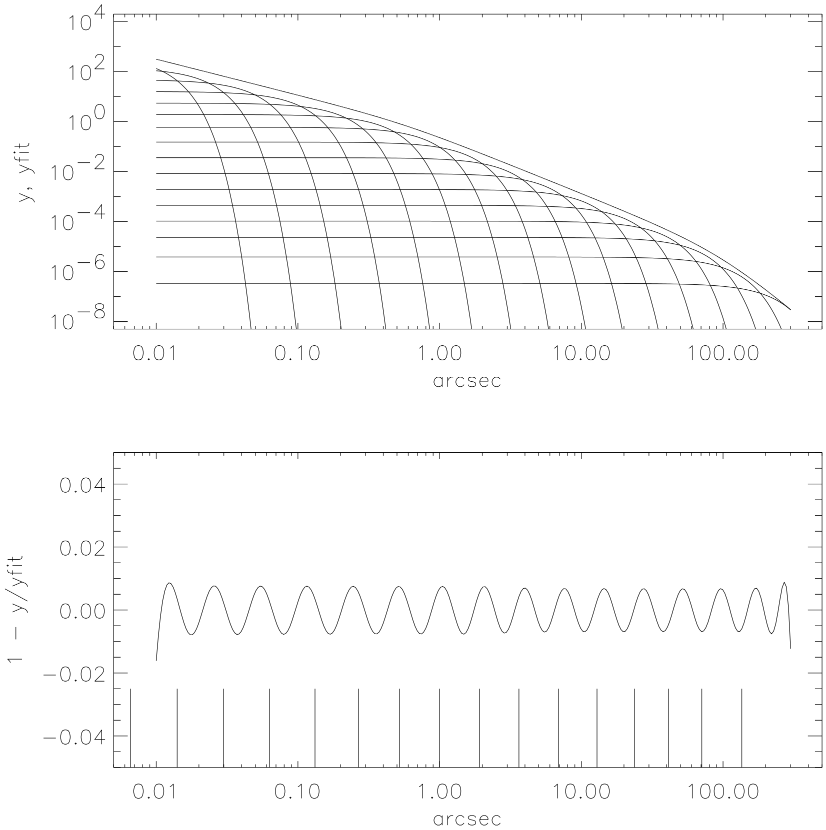

Figure 6.2: Same as in Figure 6.1 for the triple power-law profile of M32, as determined by van der Marel et al. (1998). With $N = 16$ Gaussians the maximum error is 0.7% in the range $0\farcs01$–$300''$, over ten orders of magnitude in the density.

With real photometric data the above condition for the minimax solution cannot be generally verified, due to the noise and to the undersampling in the profile. The convergence to a global solution however can still be recognized, by simple visual inspection of the result, from the fact that every Gaussian has to give significant contribution to a specific part of the profile: a Gaussian that remains always lower than any other Gaussian is generally an indication that the solution is not the global minimum (unless the profile becomes very flat).

To determine the fits of Figures 6.1–6.3 we made use of the fact that Equation (6.1) is *linear* in the Gaussians heights P_i'. It is much more efficient and accurate to separate the treatment of the linear P_i' and the nonlinear σ_i variables. In practice our 1D MGE fitting algorithm consists in the following steps:

1. we start with the σ_i logarithmically spaced in radius between the maximum $R_{\max}$ and the minimum $R_{\min}$ radius of measured photometric data. We know this is a good guess for general multiple power-law profiles;

2. we solve the nonlinear least-squares minimization problem for the σ_i, imposing the constraints that $R_{\min} < \sigma_i < R_{\max}$. The actual computation is done using the robust Levenberg-Marquardt implementation due to Moré, Garbow & Hillstrom (1980)[6]. Note

[6]We have used an IDL translation of the MINPACK-1 code by Craig B. Markwardt that is available from

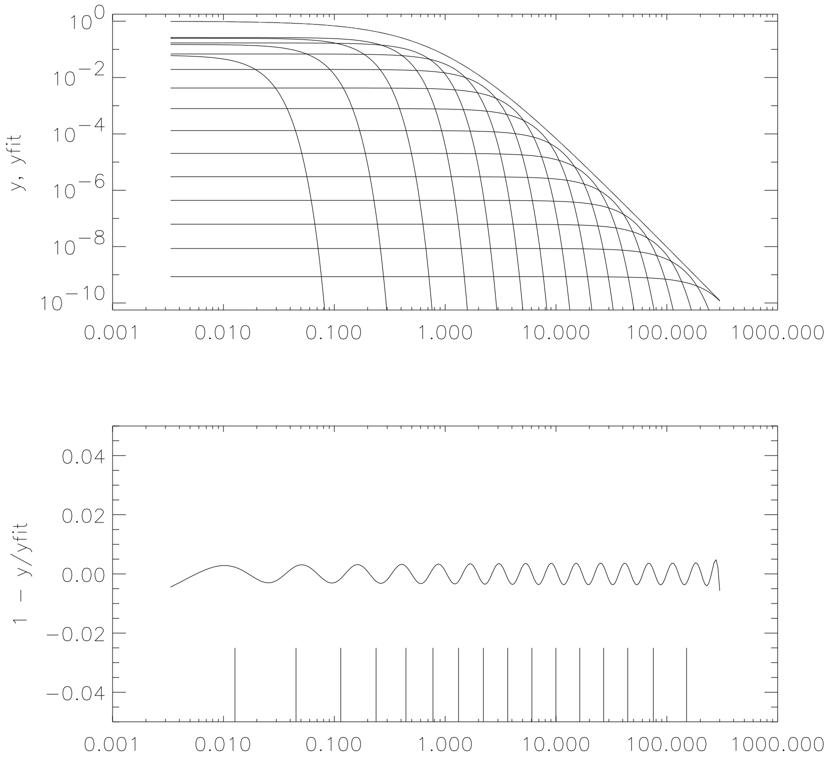

Figure 6.3: Same as in Figure 6.1 for the double power-law profile with flat core $(1+R)^{-4}$. The maximum error is 0.4% over ten orders of magnitude.

that the adopted implementation accepts bound constraints on the variables and is able to deal with degenerate Jacobians. The latter is a necessary feature since some of the variables P_i' may be zero in the final solution;

3. for every choice of the σ_i variables, during the above iterative optimization process, we find the best fit value for the P_i', with the constraints $P_i' \geq 0$. This is a Non-Negative Least-Squares (NNLS) problem that can be efficiently solved using the Lawson & Hanson (1974) algorithm[7].

In Figure 6.4 it is shown that the maximum relative error in an MGE fit to multiple power-law profiles decreases almost exponentially with increasing number of Gaussians. This is not surprising, given that every Gaussian diverges exponentially from the power-law starting from the point of closest approach. Although the actual numbers will depend on the profiles and on the adopted radial ranges, these examples give an idea of the number of Gaussians that are required to reach a given accuracy in the fit, and explain why 10–15 Gaussians generally produce a very good MGE fit to realistic Galaxy profiles. In particular in both cases the maximum relative error decreases approximately as fast as $\epsilon \propto e^{-0.4N}$.

We finally remind that, although this choice breaks somehow the elegance of the MGE parametrization, an asymptotic power-law nuclear cusp can also be imposed on the MGE

the site http://cow.physics.wisc.edu/ craigm/idl/idl.html

[7] We have translated to IDL their 1995 Fortran 90 version of the Bounded-Variables Least-Squares (BVLS) code, a generalization of NNLS.

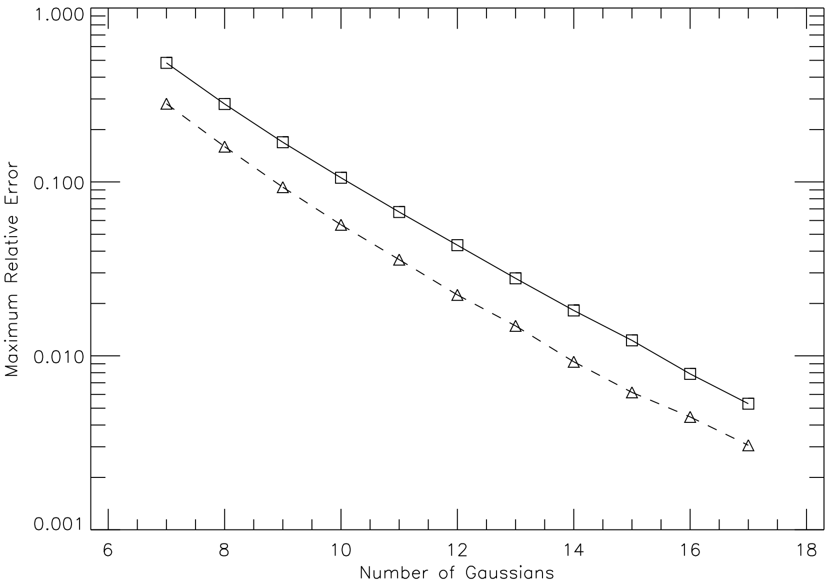

Figure 6.4: Variation of the maximum relative error in the MGE fit of Figure 6.2 (solid line) and in the fit of Figure 6.3 (dashed line) as a function of the number of Gaussians adopted in the expansion.

profile as described in Emsellem et al. (1999). This detail does not change in any way the essence of the previously described fitting algorithm.

6.2.3 Extension of the 1D Algorithm to 2D Images

In this section we extend the 1D algorithm described above to the fit of actual 2D images. We perform this extension by starting from the obvious requirement that the 2D algorithm provides *exactly* the same results of the 1D case (to be precise the same P'_i and σ_i) when it is used to fit a 2D image that presents the same major axis profile of the 1D case and has perfectly elliptical isophotes with constant axial ratio q' and position angle.

This goal is achieved by fitting "in parallel" the MGE model of Equation (6.1), simply rewritten in polar coordinates

$$\Sigma(R,\theta) = \sum_{i=1}^{N} P'_i \exp\left\{-\left(\frac{R}{2q'\sigma_i}\right)^2 \left[1 + q'^2_i + (1 - q'^2_i)\cos 2\theta\right]\right\}, \tag{6.4}$$

to a certain number $N_{\rm sec}$ of photometric profiles (all including the central pixel[8]), measured along sectors uniformly spaced in angle from the major axis to the minor axis (sectors in the four quadrants are averaged together if possible). The sampling of the photometry along the sectors is now logarithmically spaced in the elliptical radius $m^2 = x^2 + y^2/q'^2$, where q' is an average axial ratio of the galaxy isophotes (see Figure 6.5). This latter detail ensures that the requirement stated in the previous paragraph is precisely satisfied also for flattened objects. The actual photometric measurements are obtained by selecting sets of pixels on the image,

[8]A radius $R_{\rm min} = [\sqrt{2} + \sinh^{-1}(1)]/6 \simeq 0.38$ pixels has been assigned in the profiles to the central pixel, corresponding to the unweighted average radius measured from the center of the pixel.

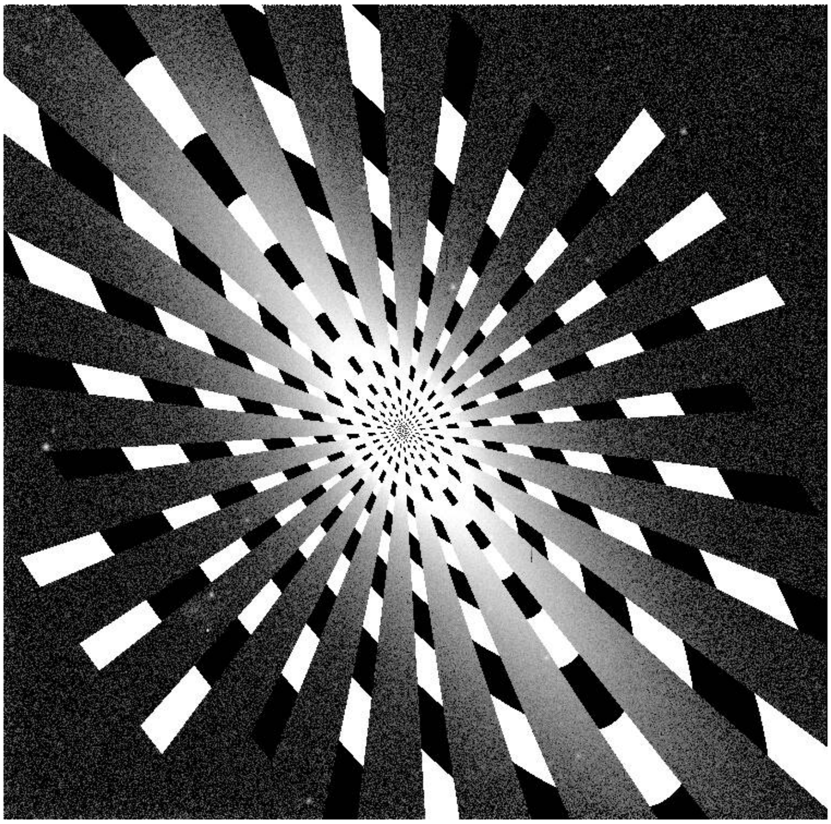

Figure 6.5: This image illustrates the sectors that have been used to produce an MGE model for the WFPC2/F814W image of the flattened S0 galaxy NGC 4342. In this example the adopted $N_{\rm sec} = 7$ sectors have a width of 5° and are spaced in angle by 15°. Note that the radial sampling of the sectors follows a characteristic isophote of the galaxy. The $35'' \times 35''$ PC1 image of the galaxy is visible in the background.

based on their angular position and logarithmic radius ranges. In the fit the same relative error is assigned to all measurements as in the 1D case, following Equation (6.3).

With these choices, when fitting a galaxy with slowly varying ellipticity with radius (as is often the case for single component objects like Ellipticals), if the input guess q' for the axial ratio is close to the galaxy average value, the procedure essentially reduces to $N_{\rm sec}$ 1D similar fits and will converge very quickly by varying almost only the σ_i as done in the previous paragraph. If the axial ratio is not constant or the isophotes are not ellipses (as in the case of spirals), both the σ_i and q'_i will have to be optimized together. In practice we still apply steps (1) and (2) of Section 6.2.2, with the only difference that we also fit the nonlinear parameters q'_i in step (1). To make the fit more robust, bound constraints are given on the variables: $R_{\rm min} < \sigma_i < R_{\rm max}$ and $0.05 < q'_i < 1$. Experience on a number of complex objects has shown that the above procedure will still converge very quickly and automatically to an excellent MGE fit to the photometry, since the initial guess for the solution is already good enough to permit to the Levenberg-Marquardt optimization algorithm to converge to the true minimum.

As an example we present an MGE fit to the “difficult” S0 galaxy NGC 4342, which has a small nuclear stellar disk, in addition to his main outer disk (van den Bosch et al., 1998). In

Figure 6.6 are presented the profiles of our best 11 Gaussians MGE fit to the WFPC2/F814W image of this galaxy, obtained with $N_{\rm sec} = 7$. A comparison between the contours of our MGE model and of the image is shown in Figure 6.7. An example of the results for the MGE fit to a more easy one-component Elliptical galaxy is shown in Figure 5.4. In this case the Gaussians succession is very regular and predictable, as in the 1D MGE fits previously discussed in Section 6.2.2.

We notice that the adopted approach also has the advantage that it is very simple to fit together multiple photometric profiles obtained from different images and even obtained from published photometry. In fact during the fit the program simply needs to know the measured values of the surface brightness and the corresponding polar coordinates, and does not have to deal with multiple images directly. In general a good fit is obtained in less than one minute on the same machine that took many hours to obtain a worst fit with the brute force approach.

6.2.4 A Fully Linear Alternative 2D Algorithm

An alternative approach to the 2D MGE fit of an image, using Gaussians with the same position angle and the same center, consists in transforming the whole problem into a NNLS problem, that can be solved with the *ad-hoc* Lawson & Hanson (1974) algorithm. This can be done by generating a large grid of all possible Gaussians that may end up in the final solution. We sample σ_i logarithmically with $R_{\rm min} < \sigma_i < R_{\rm max}$; for every choice of σ_i we sample q'_i linearly with $0.05 < q'_i < 1$. This approach is memory intensive since a copy of the data has to be kept in memory for every Gaussian in the grid: a 100×100 grid requires 10^4 copies of the photometric data, yet it is already feasible if only the profiles are used.

The advantage of this method is that it is *guaranteed* to find the best solution (although it may not be unique) within the accuracy imposed by the adopted grid of Gaussians. A big disadvantage is that in practice many more Gaussians are used by the NNLS algorithm to produce a fit with the same χ^2 that is found with our nonlinear algorithm of Section 6.2.3. This is in general an important point, since one often needs to use the MGE parametrization to perform subsequent calculations whose speed depend on the number of Gaussians: the computation of the potential scales linearly with the number N of Gaussians, while for example the solution of the Jeans equations scales as N^2 (Emsellem et al., 1994).

As an example we have used a 100×100 grid of (σ, q') values (10^4 Gaussians) to produce an MGE model for NGC 4342 using the same input photometry of Section 6.2.3. The NNLS algorithm gave a best solution with 38 positive Gaussians and an error only slightly smaller than that of the 11 Gaussians nonlinear solution of Figure 6.6 (RMS error of 0.018 mag, to be compared with 0.021 mag for the nonlinear solution).

Since the NNLS solution is ill-conditioned it may be possible to extract a subsample from the 38 Gaussians that gives essentially the same $\chi^2_{\rm best}$ of the best solution. In particular one would like to find the *smallest* set of Gaussians that still verifies $\chi^2 < (1+\epsilon)\,\chi^2_{\rm best}$, where ϵ represents a chosen fractional tolerance. Unfortunately this is a combinatorial minimization problem whose exact solution would require (today) a very large amount of time even with 38 Gaussians. We have thus adopted the following approximate method:

1. solve the NNLS problem obtained by fitting the whole (σ, q') grid of Gaussians G_j to the photometric data and define $\chi^2_{\rm best} = \chi^2$;

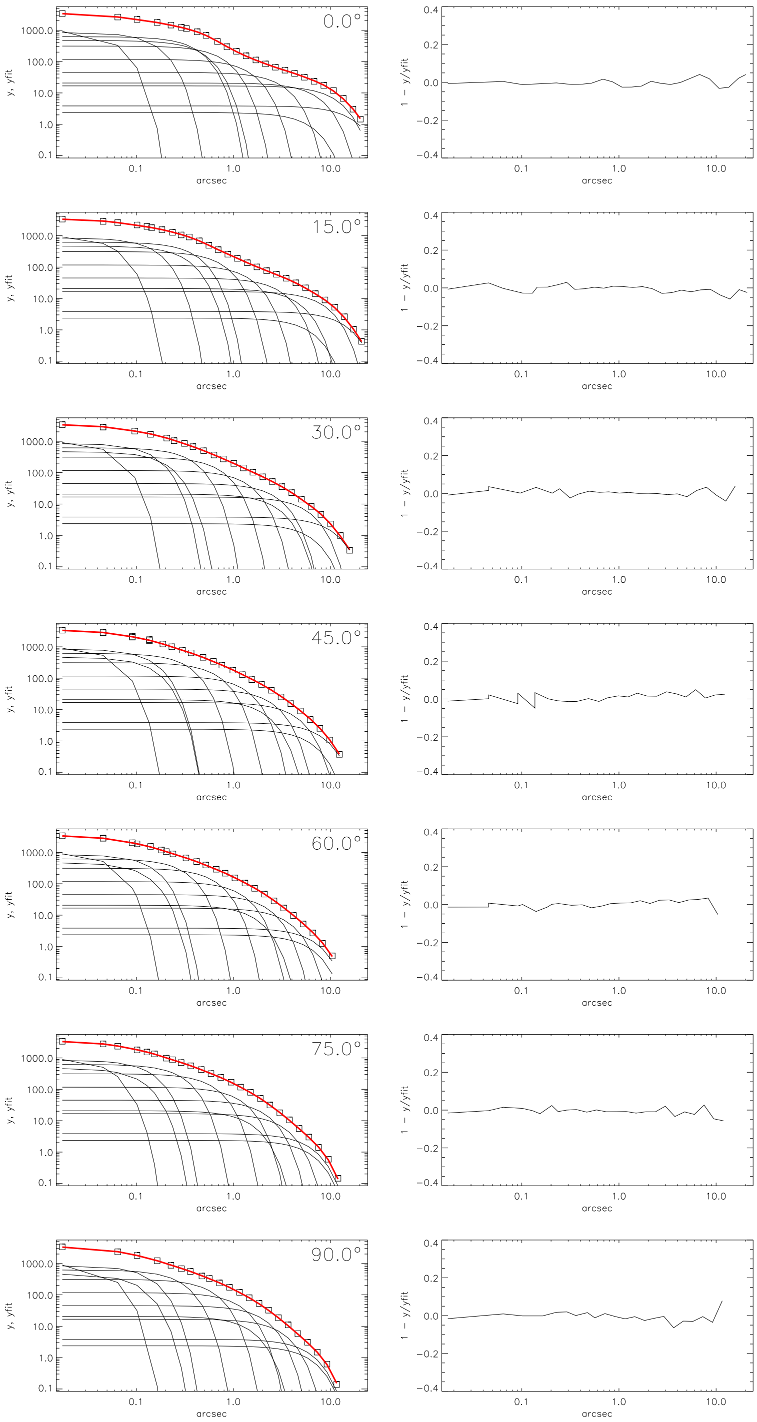

Figure 6.6: *Left Panels:* Comparison between the WFPC2/F814W photometry of NGC 4342 and the corresponding MGE best fit model. From top to bottom the profiles are measured along 5° wide sector, linearly spaced in radius between the major (0°) and the minor axis (90°). *Right Panels:* radial variation of the relative error along the profiles: the RMS error is 0.02 mag.

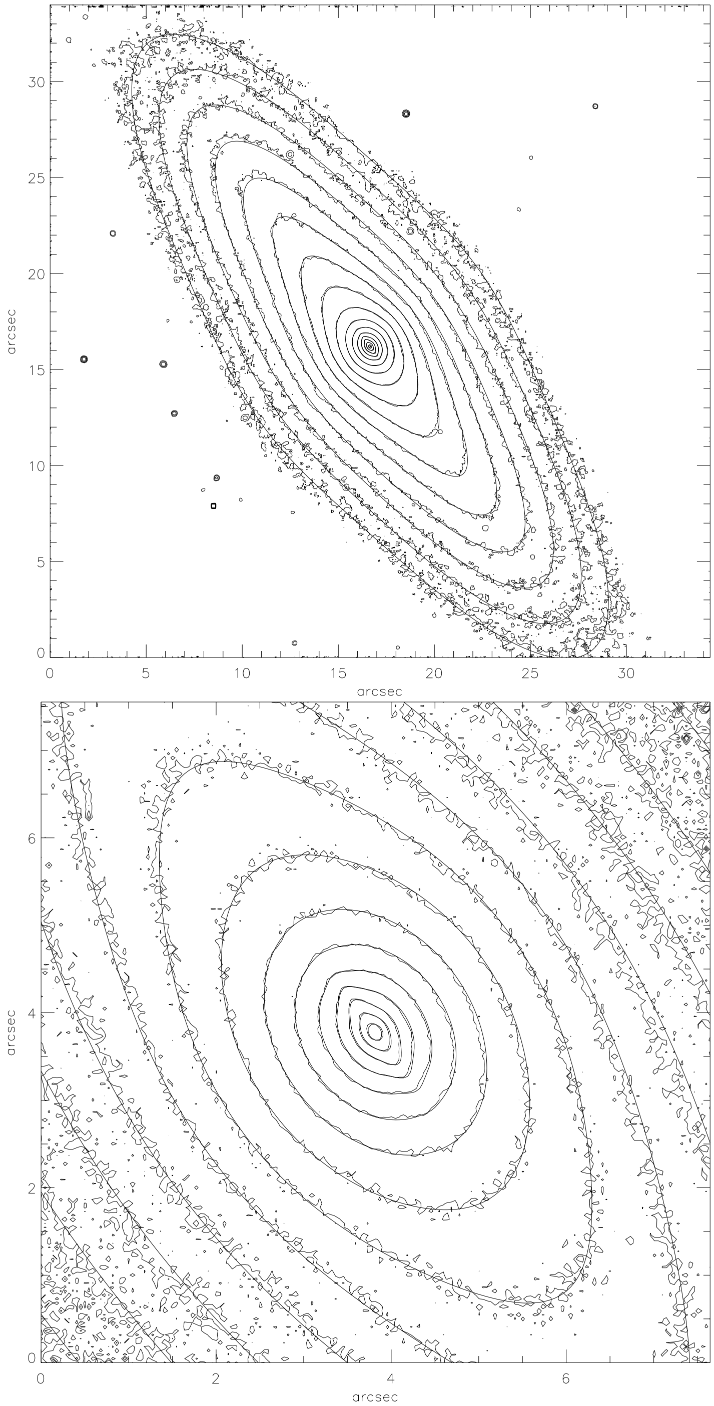

Figure 6.7: Contour maps of the WFPC2/F814W (I-band) image of NGC 4342 at two different scales: $34'' \times 34''$ (*top panel*) and $8'' \times 8''$ (*bottom panel*). Superimposed on the two plots are the contours of the intrinsic MGE surface brightness, convolved with the WFPC2 PSF. Compare this figure with Figure 1 in Cretton & van den Bosch (1999).

Table 6.1: The modeled galaxy sample

Galaxy	Revised Hubble Type	Filter	Exposure Time (s)
IC 1459	E3	F814W	460
NGC 221	cE2	F814W	1280
NGC 3379	E1	F814W	1340
NGC 4258	SAB(s)bc	F791W	1000
NGC 4261	E2	F791W	800
NGC 4342	S0	F814W	200
NGC 4374	E1	F814W	520
NGC 4486	E0pec	F814W	2430
NGC 6251	E	F814W	1000
NGC 7052	E	F814W	1400

2. construct a set S containing the positive Gaussians G_j from the previous solution, with $j = 1, \ldots, P$;
3. for $j = 1, \ldots, P$ solve a new NNLS problem, excluding G_j from S, and record the χ_j^2 obtained in the solution. Define $\chi_{j,\min}^2 = \min\{\chi_1^2, \ldots, \chi_P^2\}$;
4. if $\chi_{j,\min}^2 < (1+\epsilon)\ \chi_{\rm best}^2$, where ϵ is the maximum accepted fractional error in χ^2, then eliminate G_j from S, update the number $P \leftarrow P-1$, and go back to step (3), otherwise return S.

Running the above fully linear algorithm, we have been able to find (in a time 400× longer) a set of 14 Gaussians that produced a χ^2, in the NGC 4342 fit, non larger than that of the 11 Gaussians nonlinear solution. In general we have found that this linear algorithm is not competitive, both in speed and number of Gaussians for a given χ^2, with the one described in Section 6.2.3. Its extreme robustness however is very attractive and it can be very useful to test that a given solution cannot be significantly improved, or in cases where the final number of Gaussians is not an issue. We are exploring the possibility of performing the above combinatorial minimization step using specific algorithms like e.g. Simulated Annealing methods (e.g. Press et al., 1992), to try to decrease the number of Gaussians even further.

6.3 Tests of the Method

In the following Figures we present some tests of the algorithm described in Section 6.2.3 on a relatively large sample of galaxies. With the plan to use these data in a future application we have selected the Sample A in Ferrarese & Merritt (2000) of galaxies with high accuracy Black Hole mass determinations. The instrumental configuration of the I-band WFPC2 images used in the fits are presented in Table 6.1. We have excluded from the sample the galaxy NGC 3115, for which an MGE model which also uses ground based data has been published in Emsellem et al. (1999), and the Milky Way. The MGE model for IC 1459 is presented in Chapter 5.

Finally in the example of Figure 6.16 we show what happens in the case of an object that has non-convex isophotes and for this reason necessarily cannot be reproduced by a sum

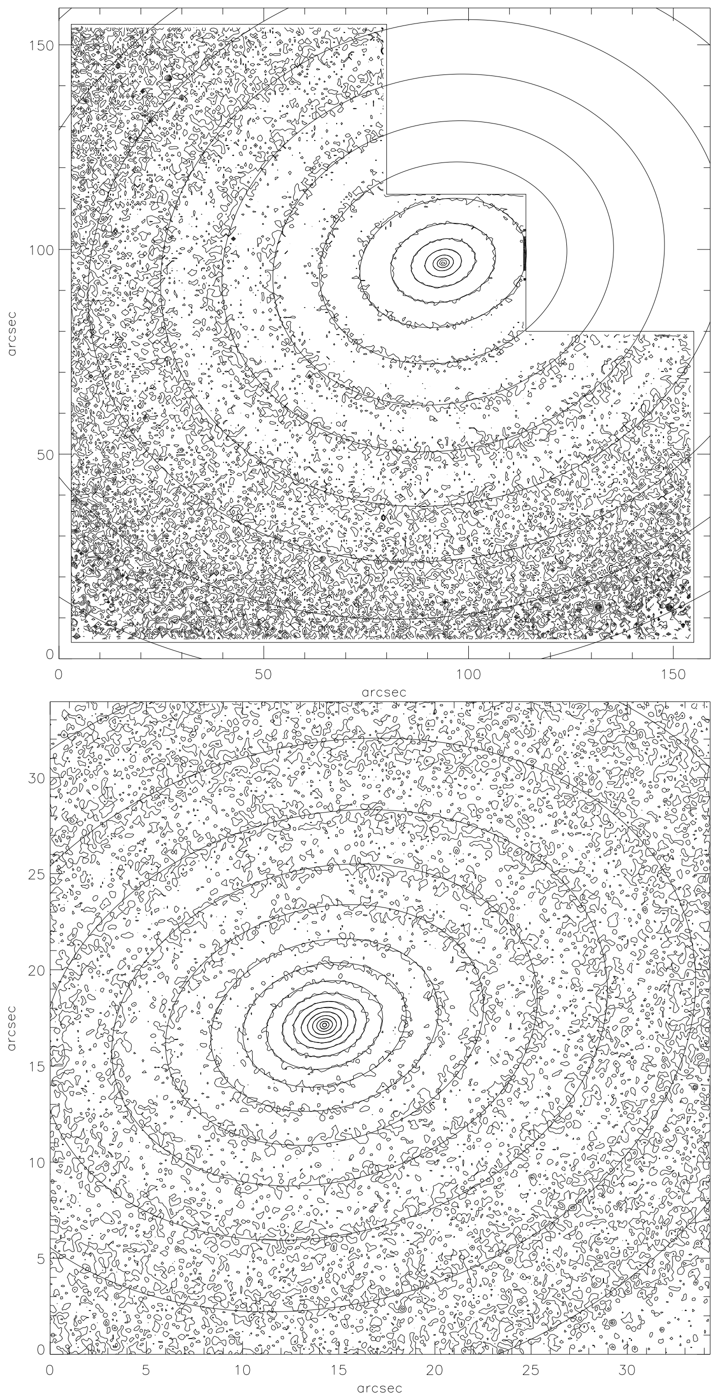

Figure 6.8: Contour maps of the WFPC2/F814W (*I*-band) image of NGC 221 (M32) at two different scales. *Top Panel:* the whole $160'' \times 160''$ WFPC2 mosaic is shown. *Bottom Panel:* the $34'' \times 34''$ PC1 CCD is presented. Superimposed on the two plots are the contours of the intrinsic MGE surface brightness, convolved with the WFPC2 PSF. The very noisy appearance of this image is due to the incipient resolution of this galaxy into stars.

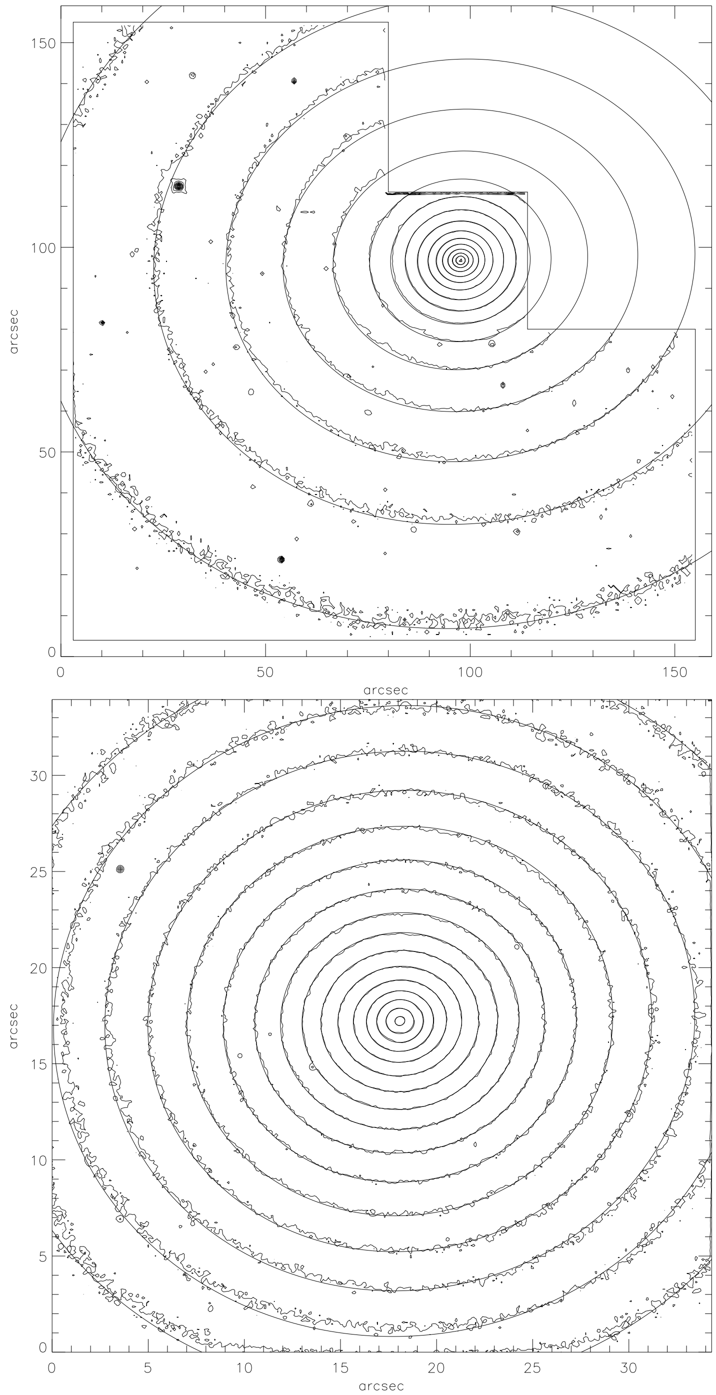

Figure 6.9: Same as in Figure 6.8 for the galaxy NGC 3379.

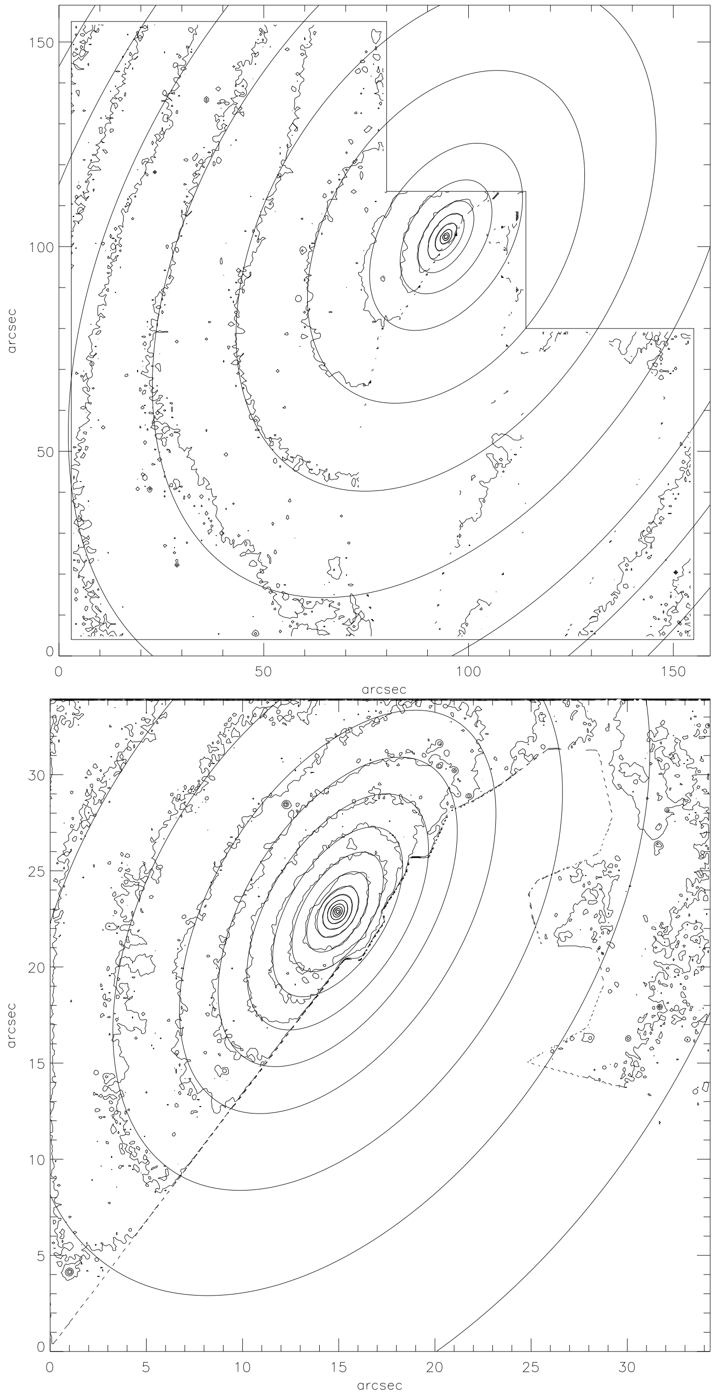

Figure 6.10: Same as in Figure 6.8 for the F791W image of the galaxy NGC 4258. Strong dust absorptions have been masked in the fit, but the galaxy also appears disturbed in the outer regions and cannot be accurately reproduced by the axisymmetric fit.

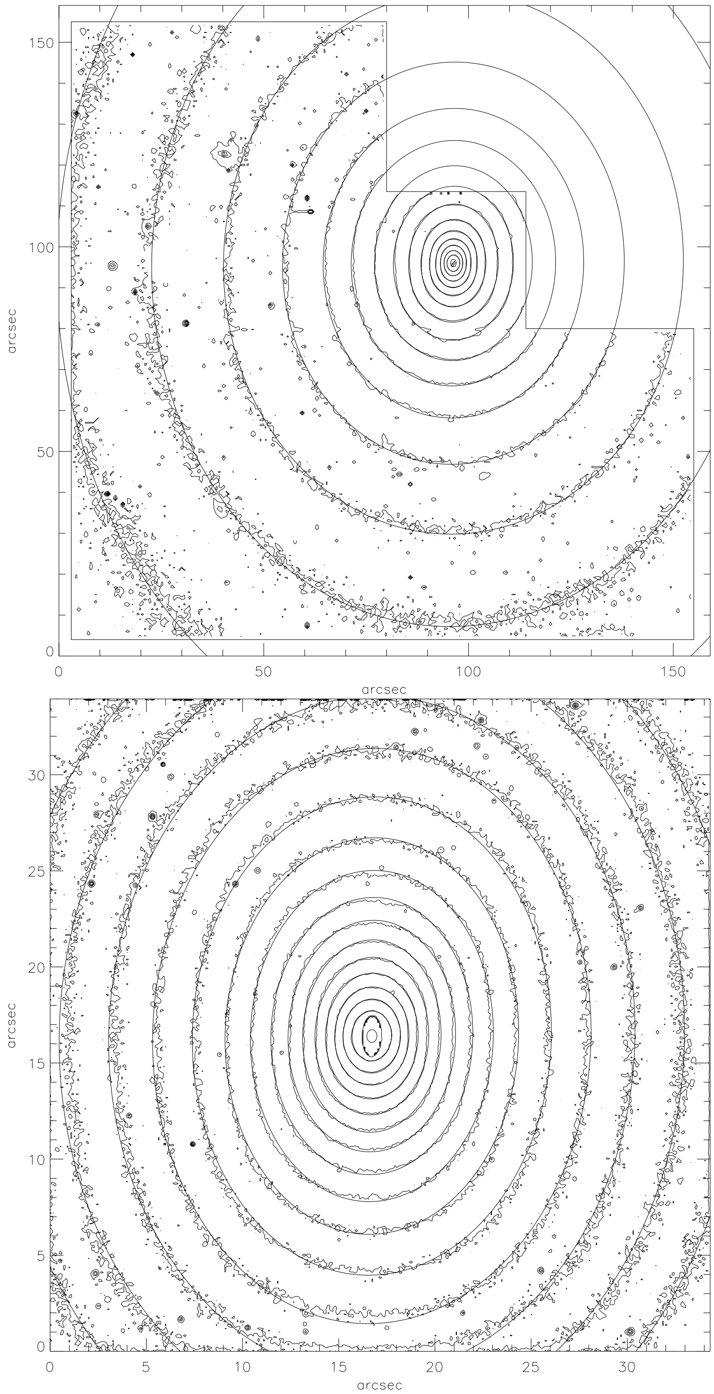

Figure 6.11: Same as in Figure 6.8 for the F791W image of the galaxy NGC 4261. The nuclear dust disk has been masked in the fit.

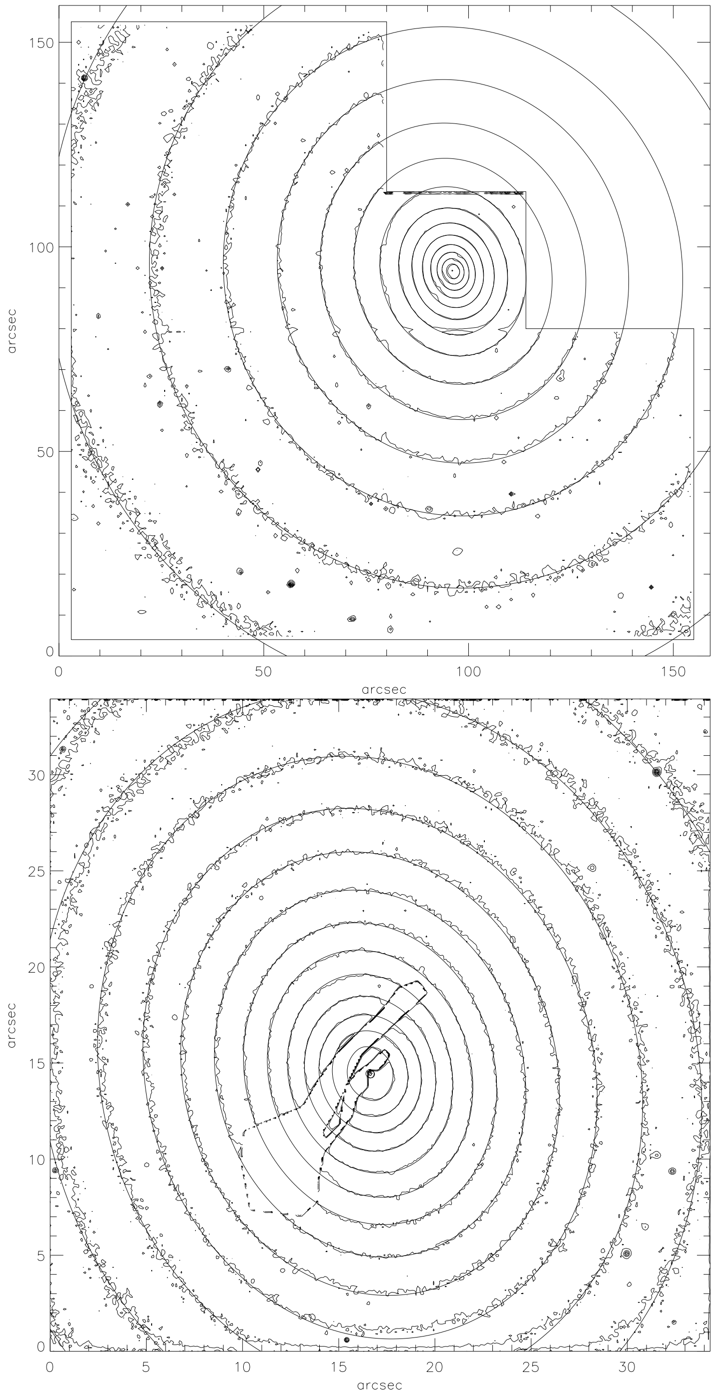

Figure 6.12: Same as in Figure 6.8 for the galaxy NGC 4374. Nuclear dust lanes have been masked in the fit.

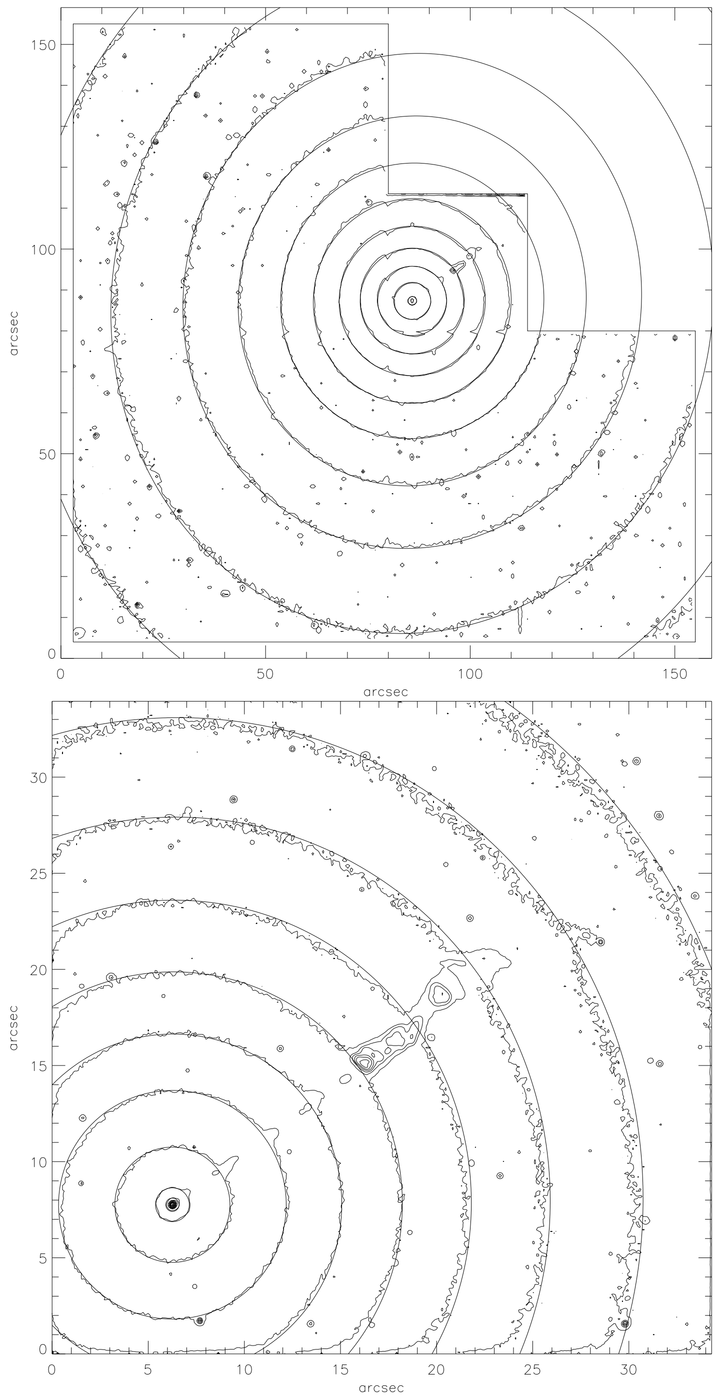

Figure 6.13: Same as in Figure 6.8 for the galaxy NGC 4486 (M87). The jet is clearly visible in this image.

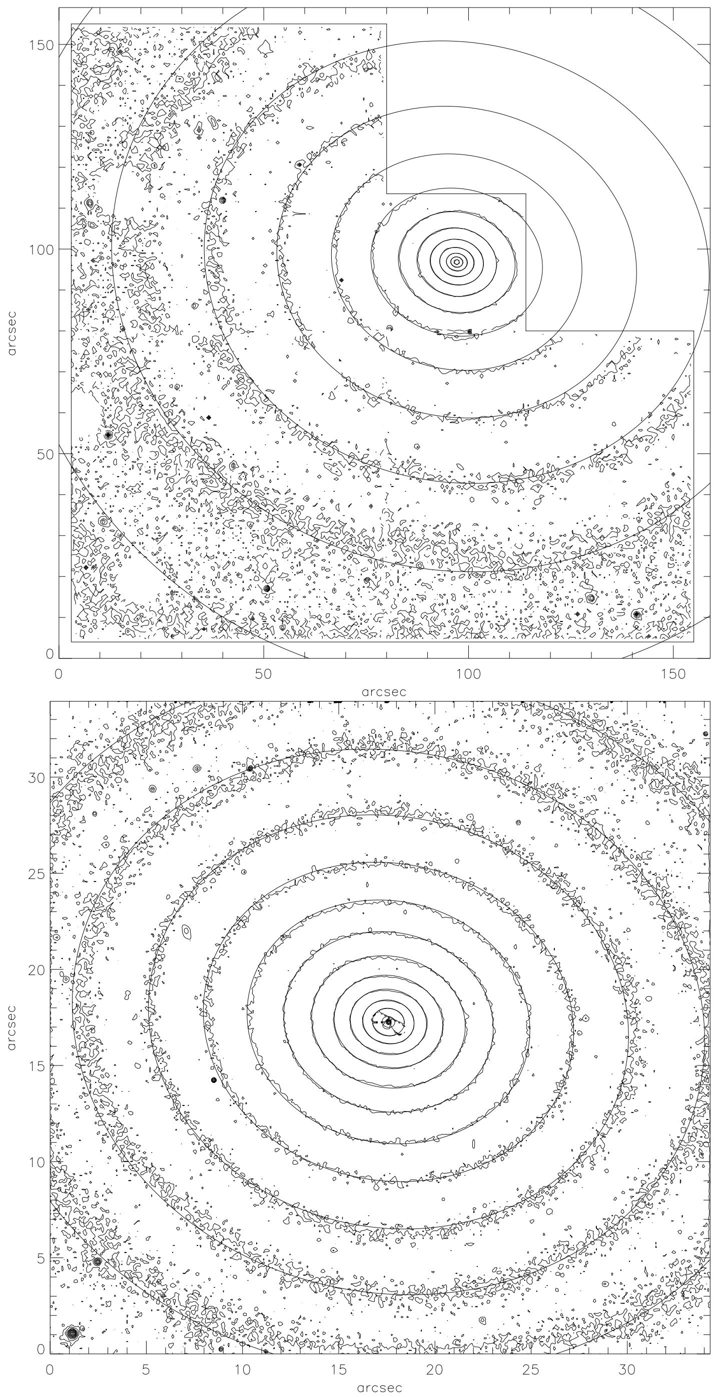

Figure 6.14: Same as in Figure 6.8 for the galaxy NGC 6251. The nuclear dust disk and some bright stars have been masked in the fit.

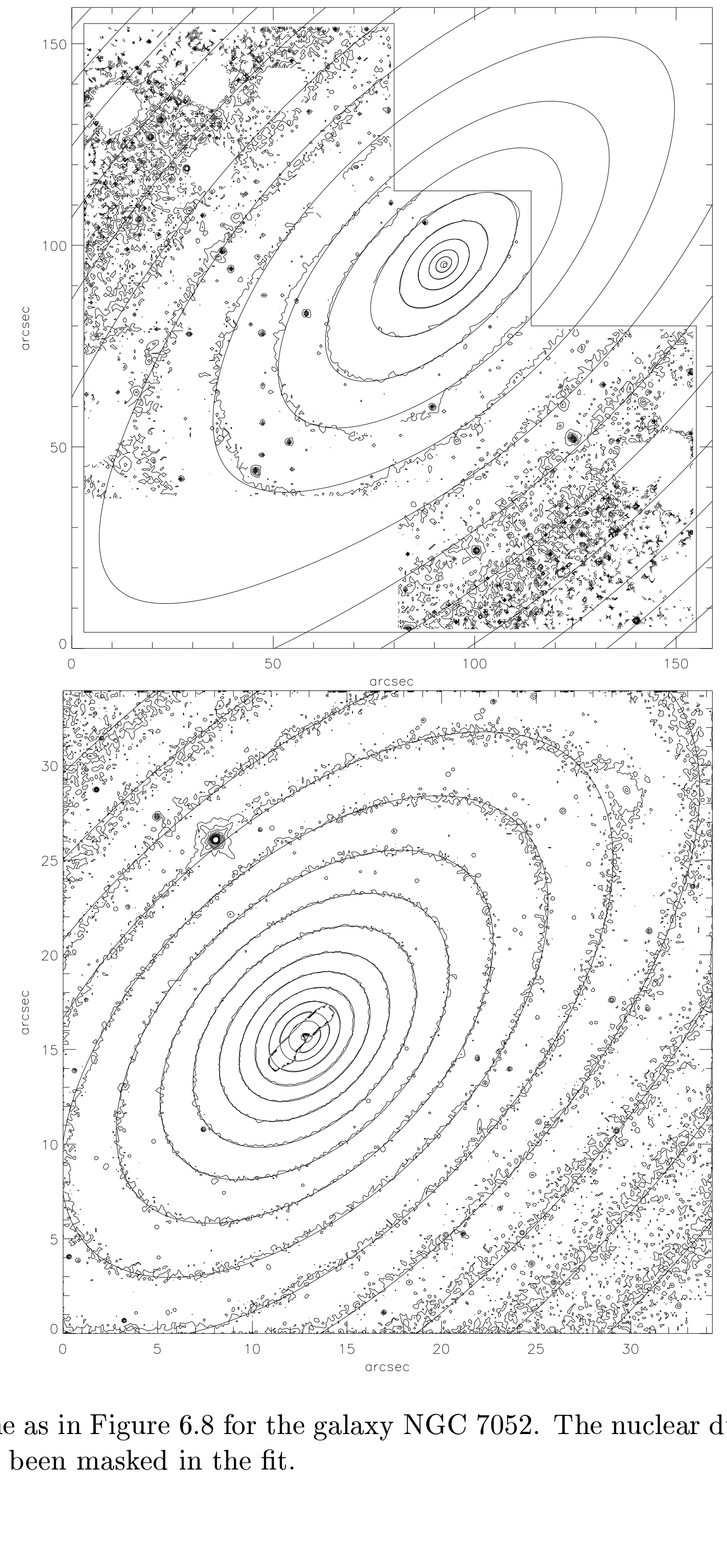

Figure 6.15: Same as in Figure 6.8 for the galaxy NGC 7052. The nuclear dust disk and some bright stars have been masked in the fit.

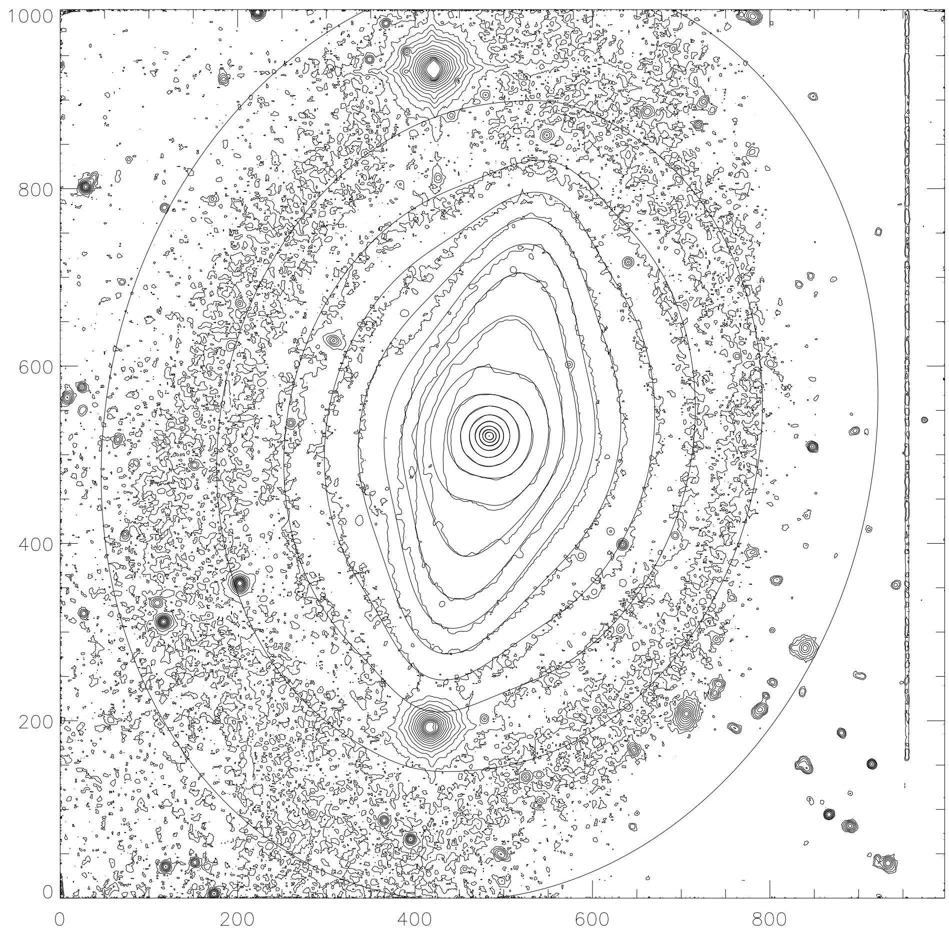

Figure 6.16: Contour plot of a V-band ground-based image of NGC 4698 obtained with the Vatican Advanced Technology Telescope. Superimposed are the contours of the best fit MGE model for this galaxy, obtained without imposing the usual positivity constraints on the Gaussians. Only in this way also the non-convex central isophotes, due to the disk profile decreasing towards the center, can be reproduced. The Gaussians reproducing the bulge in the MGE model for this image are almost perfectly round. The field of view is of $300'' \times 300''$. The dust lanes in the left part of the image have been masked during the MGE fit. This object is studied in detail in chapter 7.

of *positive* Gaussians. The non-convex isophotes of this object are due to the disk whose surface brightness decreases towards the center (see Chapter 7). By eliminating the positivity constraint on the Gaussians a good solution can still be obtained.

We stress that, after the masking of bad regions, and after specifying the common center and position angle of the Gaussians, *all* the fits have been performed in batch mode without any user intervention in less than one minute per image on a 333 MHz PC.

6.4 Conclusions

We have described a simple yet powerful algorithm that reduces the process of generating an MGE fit of a galaxy image (with constant position angle) to a simple, fast and automatic task. We have provided examples of its practical use and have tested it by accurately reproducing the photometry of a relatively large sample of galaxies observed with the WFPC2 on HST, and by comparing it with previously obtained results.

This algorithm has been implemented in an actual IDL program that can produce an MGE model starting from the original reduced images, requiring the user to only input the coordinates of the center, the galaxy position angle and a characteristic flattening of the galaxy. Multiple resolution images (e.g. ground based and HST) can easily be fitted together, in one single step.

We have also described an alternative algorithm that, although currently less practical, is guaranteed to converge to the minimum χ^2 solution within the accuracy imposed by an adopted grid of parameters in the solution space.

Both algorithms can be in principle naturally extended to the case of non axisymmetric galaxies with varying isophote position angle, once the triaxial dynamical codes requiring them will be available. The complete IDL source code implementing the algorithm described in this Chapter, together with usage examples, will be available from the author upon request.

Acknowledgments

I am grateful to José Funes and Alessandro Pizzella for obtaining the CCD image shown in Figure 6.16 and to Claudia Scarlata for providing us with a reduced version of this image.

Bibliography

Bendinelli, O. 1991, ApJ, 366, 599

Byun, Y.-I. et al. 1996, AJ, 111, 1889

Cretton, N., & van den Bosch, F. 1999, ApJ, 514, 704

Emsellem, E., Monnet, G., & Bacon, R. 1994, A&A, 285, 723

Emsellem, E., Monnet, G., Bacon, R., & Nieto, J.-L. 1994a, A&A, 285, 739

Emsellem, E. 1995, A&A, 303, 673

Emsellem, E., Bacon, R., Monnet, G., & Poulain, P. 1996, A&A, 312, 777

Emsellem, E., Dejonghe, H., & Bacon, R. 1999, MNRAS, 303, 495

Ferrarese, L., & Merritt, D., 2000, ApJ, 539, L9

Gebhardt, K. et al. 1996, AJ, 112, 105

Hunter C., & Qian E. 1993, MNRAS, 202, 401

Lauer, T. R. et al. 1995, AJ, 110, 2622

Lawson, C.L., & Hanson, R. 1974, Solving Least Squares Problems; 1995, 2nd ed. (Englewood Cliffs, NJ: Prentice-Hall)

Monnet, G., Bacon, R., & Emsellem, E. 1992, A&A, 253, 366

Moré, J.J., Garbow, B.S., & Hillstrom, K.E. 1980, User Guide for MINPACK-1, Argonne National Laboratory Report ANL-80-74

Press, W. H., Teukolsky, S. A., Vetterling, W. T., & Flannery, B. P. 1992, Numerical Recipes in FORTRAN 77 (2d ed; Cambridge: Cambridge Univ. Press)

Rybicki, G. B. 1986, in Structure and Dynamics of Elliptical Galaxies, ed. P.T. de Zeeuw (Dordrecht: Reidel), 397

van den Bosch, F.C, Jaffe, W., van der Marel, R.P. 1998, MNRAS, 293, 343

van der Marel, R.P., Cretton, N., de Zeeuw, P.T., & Rix, H. 1998, ApJ, 493, 613